Applied Geochemistry 23 (2008) 3072–3087

Contents lists available at ScienceDirect

Applied Geochemistry

journal homepage: www.elsevier.com/locate/apgeochem

Groundwater flow in an arsenic-contaminated aquifer, Mekong Delta, Cambodia

Shawn G. Benner [a,*], Matthew L. Polizzotto [b], Benjamin D. Kocar [b], Somenath Ganguly [a], Kongkea Phan [c], Kagna Ouch [c], Michael Sampson [c], Scott Fendorf [b]

[a] Department of Geosciences, Boise State University, Boise, ID 83705, USA
[b] School of Earth Sciences, Stanford University, Stanford, CA 94305, USA
[c] Resource Development International, Kien Svay, Kandal, Cambodia

ARTICLE INFO

Article history:
Available online 4 July 2008

ABSTRACT

To advance understanding of hydrological influences on As concentrations within groundwaters of Southeast Asia, the flow system of an As-rich aquifer on the Mekong Delta in Cambodia where flow patterns have not been disturbed by irrigation well pumping was examined. Monitoring of water levels in a network of installed wells, extending over a 50 km^2 area, indicates that groundwater flow is dominated by seasonally-variable gradients developed between the river and the inland wetland basins. While the gradient inverts annually, net groundwater flow is from the wetlands to the river. Hydraulic parameters of the aquifer ($K \approx 10^{-4}$ ms^{-1}) and overlying clay aquitard ($K \approx 10^{-8}$ ms^{-1}) were determined using grain size, permeameter and slug test analyses; when coupled with observed gradients, they indicate a net groundwater flow velocity of 0.04–0.4 ma^{-1} downward through the clay and 1–13 ma^{-1} horizontally within the sand aquifer, producing aquifer residence times on the order 100–1000 a. The results of numerical modeling support this conceptual model of the flow system and, when integrated with observed spatial trends in dissolved As concentrations, reveal that the shallow sediments (upper 2–10 m of fine-grained material) are an important source of As to the underlying aquifer.

1. Introduction

There has been extensive investigation into the geochemical processes leading to elevated As in the deltaic groundwaters in Asia and there is emerging consensus that reductive dissolution of Fe oxides is an important mechanism leading to As release to the porewaters of the aquifers in the region (Nickson et al., 2000; Harvey et al., 2002; McArthur et al., 2004; Islam et al., 2004). In contrast, there has been less agreement regarding the both the role of hydrology in As release and the importance of surficial processes as a source of As and/or organic C (see Harvey et al 2002 and associated discussion). Many studies present evidence that As is released from sediments at depth (e.g. McArthur et al., 2004; Islam et al., 2004), while near-surface processes have also been evoked (Polizzotto et al., 2005; Harvey et al., 2006). Based on work at a field site in Cambodia, the authors recently proposed that significant As is mobilized from shallow sediments with release and transport strongly influenced by surface hydrologic processes and coupled groundwater flow (Polizzotto et al., 2008). A tight linkage between As behavior and hydrology implies that ongoing and future anthropogenic activities (i.e. land use change, groundwater pumping, sediment excavation) will likely influence As behavior, potentially alleviating or exacerbating this massive health crisis.

Elucidating the role of the hydrologic flow system on release (and transport) has been hampered by the flow complexity of the heavily pumped Bangladeshi aquifers where most research has been focused. Such local flow

* Corresponding author.
E-mail address: sbenner@boisestate.edu (S.G. Benner).

0883-2927/$ - see front matter © 2008 Elsevier Ltd. All rights reserved.
doi:10.1016/j.apgeochem.2008.06.013

complexity has precluded the development of a site-specific, spatially distributed flow model that can enable evaluation of changes in geochemical parameters, inclusive of As concentrations, along a constrained flow path. Despite this complexity, a number of recent observations indicate that hydrologic conditions influence the resulting distribution of dissolved As within the aquifer (Harvey et al., 2006; Klump et al., 2006; Postma et al., 2007; Stute et al., 2007).

Harvey et al. (2006) overcame the challenges of a spatially distributed modeling approach by utilizing a detailed, lumped-parameter model to demonstrate that the aquifer at their Munshiganj site in Bangladesh was rapidly flushed (residence times of <100 a), and that pumping for irrigation had altered the physical and chemical nature of the groundwater system. Furthermore, this evaluation suggested that ponds, which have been excavated into the surficial clay layer at the site, may be a primary source of recharge to the aquifer. Klump et al. (2006), also working in the Munshiganj district of Bangladesh, coupled $^{3}H/^{3}He$ groundwater dating with conceptual flow modeling to propose that the highest As concentrations are found within a zone of convergent flow produced by irrigation pumping. Similarly, Stute et al. (2007) suggest, again based on $^{3}H/^{3}He$ groundwater dating in Bangladesh groundwater, that groundwater flushing (driven by pumping) may explain the spatial distribution of As in the aquifer. At a separate site in Bangladesh, van Geen et al. (2006) demonstrated a correlation between hydraulic soil properties and the concentration of As in the underlying aquifer; areas with more sand and less clay were correlated to lower As levels. At an intensively instrumented field site on the Red River in Vietnam, Postma et al. (2007) documented steep gradients in As concentrations along flow paths in the upper 10 m of the aquifer and detailed biogeochemical changes along inferred flow paths. In Polizzotto et al. (2008), the authors proposed a tightly coupled hydrologic and geochemical model indicating that elevated As concentrations within the aquifer are, at least in part, released from shallow sediments and transported to depth by infiltrating surface water. While not exclusionary of other release processes and locations, the proposed model provides a mechanism to explain As profiles throughout the aquifer. Here, a more detailed description of the physically-based hydrological framework of groundwater flow that enabled this interpretation of observed spatiotemporal trends in groundwater geochemistry is presented. In a companion submission, the biogeochemical profiles and mechanisms leading to As release from shallow sediments are described in detail (Kocar et al., 2008).

The hydrologic complexity induced by groundwater pumping for irrigation has been overcome by developing a model for a regional scale, As-rich, deltaic aquifer in Cambodia where groundwater flow is minimally disturbed by groundwater pumping (Polya et al., 2005). Specifically, an extensive hydrologic dataset, of regional extent, has been created and interpreted using simple mass balance/flux calculations and numerical flow modeling, to develop a site-specific, spatially distributed, model of the groundwater flow system. The hydrogeology at the site is driven by dramatic, seasonally-variable fluctuations in surface water levels and is strongly influenced by a surficial clay depositional unit. It is demonstrated that, despite a seasonal reversal of flow direction, the net annual groundwater flow is downwards from wetland basins to the underlying aquifer and horizontal from the aquifer to adjacent rivers.

1.1. Field site description

The 50 km^2 field area is located on the Mekong Delta in the Kandal province of Cambodia, SE of Phnom Penh (Lat. 11 31 3.90N, Long. 105 0 41.77E, Fig. 1). The Mekong River is a broad river that carries the seventh largest sediment load in the world, the majority of which is discharged during the wet season. The site is located at the upper end of the delta and is bound by two deltaic distributaries of the Mekong River (Mekong and Bassac branches). As on the other major deltas of Asia, Mekong topography is very subdued (maximum elevation typically <10 m) and is characterized by elevated natural levees along the riverbanks receding to a native, seasonally-flooded, wetland basin between the two rivers (Buschmann et al., 2007). The sediments of the Mekong Delta were deposited over the previous 7.5 ka following the last sea level high-stand (Nguyen et al., 2000; Ta et al., 2002; Tamura et al., 2007). At the site, the sediment sequence is composed of >30 m of aquifer-forming sands overlain by approximately 15 m of silts and clays (JICA, 2002; Tamura et al., 2007). The aquifer of the low-lying Mekong floodplain in Cambodia is the primary drinking water source for much of the rural population, yet elevated dissolved As concentrations are common (Polya et al., 2005; Berg et al., 2007). Within the aquifer at the field site, dissolved As concentrations are nearly universally elevated with almost all wells within the aquifer exceeding 100 $\mu g L^{-1}$ (Fig. 2). During the study period, groundwater pumping throughout the field site was limited to domestic extraction.

2. Methods

2.1. Groundwater and surface water monitoring network

A network of 80 installed wells and 10 surface water monitoring sites are distributed throughout the field area (Fig. 1). At two locations additional near-surface lysimeters and a subset of closely spaced wells provide more detailed spatial analyses (see intensive sites, Fig. 1). At most locations outside the detailed monitoring sites, wells are installed as nested wells with one well screened across the water table within the clay unit (4–12 m), and two wells screened in the upper (20–30 m) and lower (36–60 m) portions of the aquifer sands. Wells were installed using a locally developed manually-driven, direct rotary method (1.5″, 3.8 cm, diameter pipe with a 4″, 10.2 cm, diameter open cutting tip) where a water-based slurry is pumped down the center pipe of the drill, lifting drill cuttings to the surface along the annulus between the drill pipe and drill hole. Wells are composed of 3.2 cm diameter PVC piping, typically screened over the lower 4 m. After installation, wells were backfilled with sand over the screened interval and capped with clay or cement to the surface.

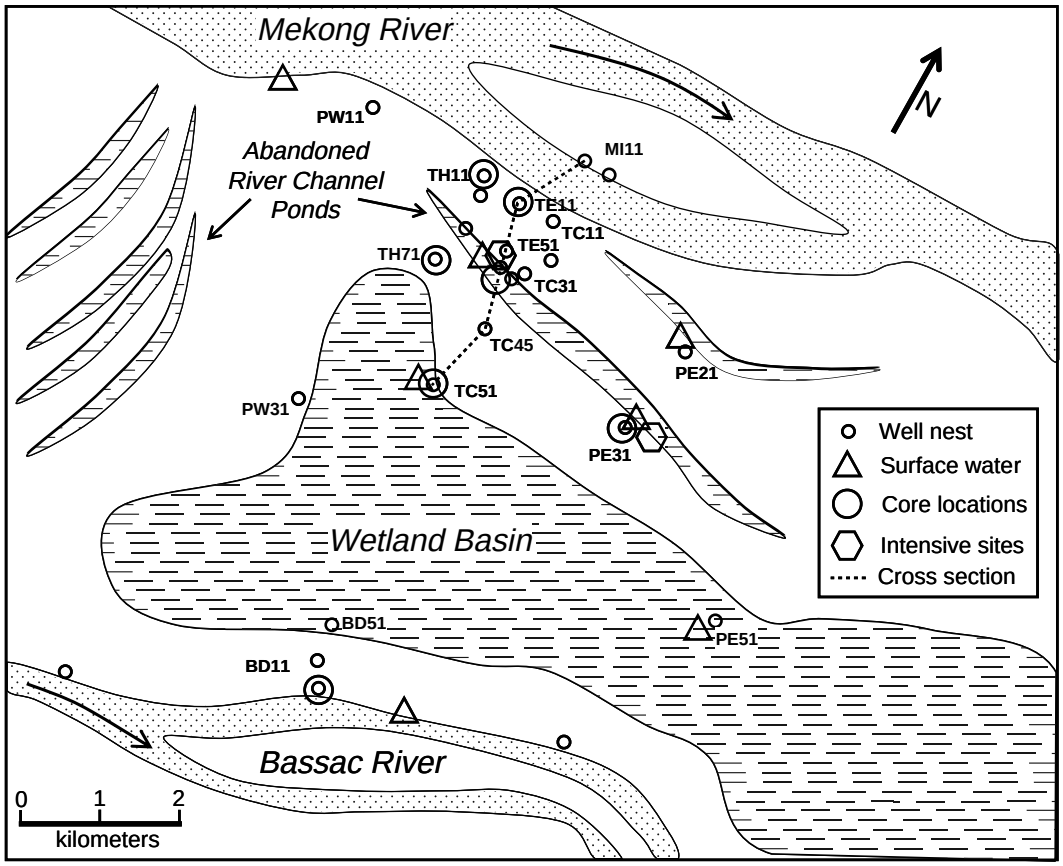

Fig. 1. Field area map. Phnom Penh, the capital of Cambodia, is located approximately 15 km to the west of the field area.

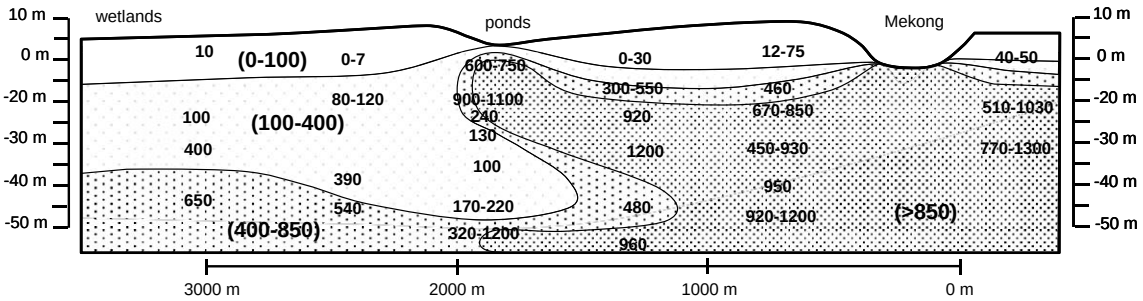

Fig. 2. Cross sectional profile along transect shown in Fig. 1, with As concentrations, all values in $\mu g L^{-1}$. The numbers in parentheses indicate the range for shaded contours. The vertical axis is expressed as meters above mean sea level (mASL).

2.2. Water levels

All reference points, wells, and surface water monitoring sites used for water level measurements were spatially linked by vertical surveying with an auto level (2.5 mm accuracy per double km run); field error was <5 mm on closed loops.

Mekong River stage levels were provided by the Mekong River Commission (MRC) and are representative of the recent historical average. Distance-weighted averages from the Phnom Penh Port (upstream of the site) and the Neak Luong (downstream) stations were used to calibrate the absolute elevation of the water level monitoring site in the Mekong River, and elevations throughout the field area were referenced with these MRC data. Hydraulic heads in each well were measured weekly with an electronic water level tape, and surface water levels were measured weekly with a weighted measuring tape from points of fixed elevation. Water levels are reported as meters above mean sea level (mASL).

2.3. Tidal monitoring

Daily, tidally-driven changes in water levels in the Mekong and within groundwater wells were measured using In-Situ Level Troll 500 and 700 Series pressure transducers. A transducer, set to record at a rate of once per minute, was placed in the Mekong approximately 2 m below the river surface. A second pressure transducer was then sequentially placed in wells TC11, TH11, and TC31 for approximately 48 h time periods, producing a series of river-aquifer paired datasets.

2.4. Stratigraphy and sediment hydraulic properties

A cross-sectional profile of the site stratigraphy (Fig. 3) was constructed by interpretation of well log data (visual and texturally-based documentation of well cuttings during well installation) and limited sediment core data (Fig. 1) and was interpreted within the constraints of the detailed sedimentary history proposed by Tamura et al. (2007). An intact coring procedure was used at selected locations for sediment retrieval. A 0.75″ (1.9 cm) open core device fitted with a polycarbonate sleeve and core-catcher was deployed through the drilling pipe at 3 m intervals and driven into the undisturbed sediment below the drilling tip. Once retrieved, samples were immediately capped and sealed in O_2-impermeable anaerobic pouches to prevent oxidation of the sediments. Sediment samples were stored and transported at 4 °C.

Particle size separation was performed on 14 aquifer sand samples and the resulting grain size distributions were used to calculate hydraulic conductivity values. The Breyer method was used to calculate hydraulic conductivities of the fine sand aquifer sediments; the Hazen method was used to obtain K values for medium and coarse aquifer sand samples, (Kresic, 1997).

Constant head permeameter tests (Domenico and Schwartz, 1998) were performed on 10 samples from the upper clay layer (composed of silts and clays), with depths ranging from 6 m to 18 m, in order to determine hydraulic conductivity values. Samples were dried and repacked into sealed flow cells, with lengths of 3.3 cm and cross-sectional areas of 24 cm^2. Constant flow was maintained and monitored. For each sample, the test was repeated at 3–6 different pressure heads; for each trial at all depths at each site, the range of calculated K values was within a factor of 2.

Slug tests were performed on 15 shallow (8–12 m) wells throughout the field area and the resulting head changes were analyzed according to the Hvorslev method (Hvorslev, 1951). The resulting K values for the falling head and rising head tests were within a factor of 2 from each other in all but one case. The results of hydraulic conductivity determination are summarized in Table 1.

2.5. Water chemistry data collection and plotting

All monitoring wells were sampled once over the time period January 2005 to March 2006. Wells were sampled and analyzed for As by inductively coupled plasma optical emission spectrometry using hydride generation. Select wells were sampled four times over the season,

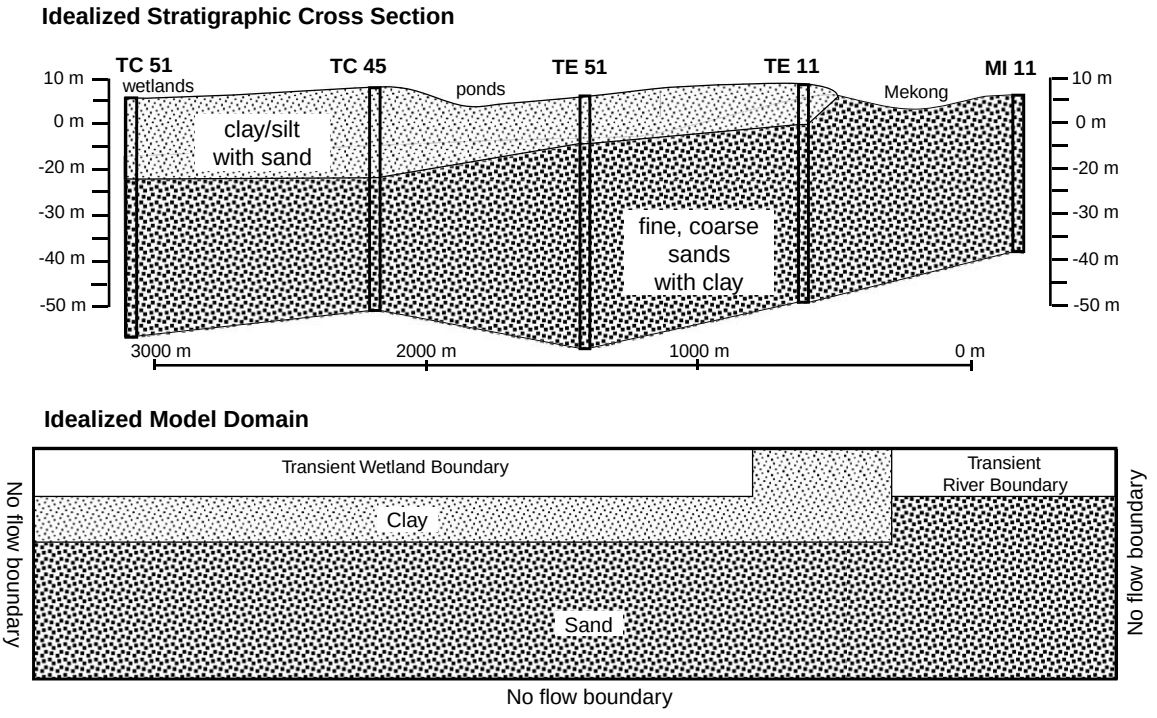

Fig. 3. Sedimentary cross-section of field area and idealized model domain (see Fig. 1 for location). The vertical axis is expressed as meters above mean sea level (mASL). The model domain is 4000 m (400 cells) × 60 m (20 cells).

Table 1
Hydraulic conductivities for aquifer sand and surface clay sediments, based on grain size analysis, constant head permeameter testing and slug test analysis

Method	Aquifer sands	Surface clays	
	Grain size	Permeameters	Slug tests
Average K (ms^{-1})	3.15E−04	4.08E−07	1.22E−06
Standard deviation (ms^{-1})	3.02E−04	5.94E−07	1.89E−06
Median K (ms^{-1})	2.70E−04	5.02E−08	4.76E−07
Number of samples	14	10	15

establishing that there was little variation in concentration within the aquifer. The exception was observed temporal variations in the recharge and discharge zones. Collected data from multiple transects was projected onto a single plane based on distance-from-the-river. The resulting two dimensional, cross-sectional, plot of the data was then contoured using visual interpolation.

2.6. Numerical modeling

Numerical modeling was undertaken to further evaluate and refine (or revise) the emerging groundwater flow conceptualization. Model calibration was conducted by seeking to reproduce the seasonal trends in hydraulic heads observed in the monitoring wells within the aquifer. Aquifer properties were constrained by field-measured or documented literature values. It was also sought to produce a net average flow field consistent with that dictated by the measured annual gradients. In practice, this entailed adjusting the hydraulic conductivity values of the clay and the sand (within the constraints of the observed range of values) to optimize the relative influence of the seasonal wetland and river hydraulic head changes on the aquifer wells.

Numerical modeling was conducted using MODFLOW and MODPATH (McDonald and Harbaugh, 1988) under both transient and steady-state (net annual) conditions. Simulations were conducted in a two-dimensional cross-sectional grid (60 m, 20 cell depth; 4000 m, 400 cell width, Fig. 3). An assumption of symmetry between the Bassac and Mekong Rivers enabled the establishment of a no flow boundary at the center of the wetlands and the middle of the Mekong River. The base of the aquifer (assumed to be at 60 m depth) was also designated a no flow boundary condition. Transient boundary conditions were defined by a fitted function of the 5 day running average of measured water wetland/pond and river levels over the time period from January 2005 to March 2006 (Fig. 4). These boundary conditions were represented by cells 12 m thick to accommodate seasonal head fluctuations. The hydraulic conductivity field was expressed as a simplified 2-layer system with 13 m of clay overlying 36 m of sand.

Material properties were fixed based on field and literature values (Table 2) with the exception of hydraulic conductivity values, which were treated as the primary variables during transient model calibration. The range of hydraulic conductivity values was constrained by the range of field-measured values and by the observed gradients across the clay (between the wetlands and the aquifer) and across the sand (aquifer to the river).

Model calibration was conducted by adjusting hydraulic conductivity values for the clay and sand to reproduce field-observed temporal trends (both seasonal and daily-tidal) in well water levels at varying distances from the Mekong River. The assumption of two-dimensionality (i.e. all flow perpendicular to the river) was evaluated by comparing the model results with observed trends along parallel well transects.

The resulting hydraulic conductivity values were used in steady-state (annual average) flow simulations in which

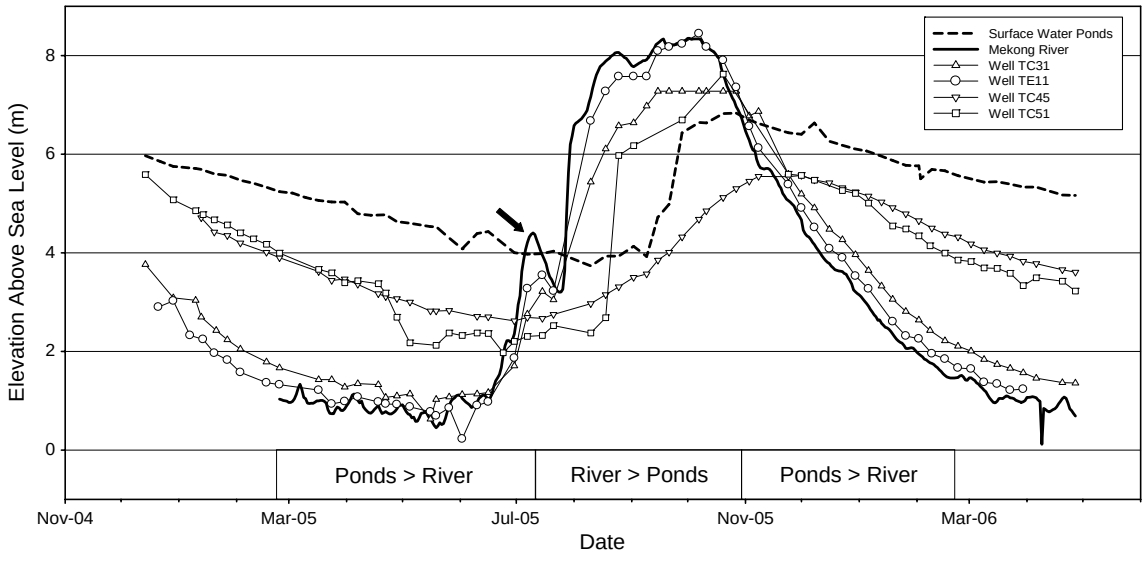

Fig. 4. Seasonal Mekong River, wetland and well hydrographs. Arrow indicates distinct river hydrograph peak that is observed in groundwater wells and captured in numerical modeling results.

the wetland and river heads were fixed to produce the observed average annual head differences.

3. Results and discussion

3.1. Stratigraphy

Throughout the field area, a silt-clay aquitard overlying the sand aquifer was observed at all drill locations (Fig. 3). While drilling and coring techniques did not permit collection of continuous, undisturbed cores, the observed stratigraphy is consistent with the sedimentary profile and history of the upper Mekong Delta proposed by Tamura et al. (2007). The upper silt/clay unit ranges in thickness from 5 to 22 m, is typically orange colored at the surface, and is green to grey at its base. Carbon dating of this fine-grained sequence indicates that the entire unit was deposited over the previous 7.5 ka; the upper, orange colored sediments were likely deposited over the previous 0.7 ka (Tamura, 2007). Below the upper clay/silt unit, a distinct transition to sand-rich sediments is observed. The aquifer sand unit extends from an average depth of 15 m to the maximum depth of drilling (60 m), and this unit is characteristically fine to course grained, is grey in color, and contains clay lenses. Near the base of the sand unit at some locations (particularly proximal to the Mekong and Bassac Rivers), coarse grained sands and gravels are observed. Depth to bedrock is, however, poorly constrained. Based on ground-penetrating radar analyses, JICA (2002) estimated that consolidated bedrock ranges from 120 to 160 m below the surface throughout the upper delta region (JICA, 2002), but this has not been confirmed by geophysics nor drilled wells in the field area. In fact, one JICA borehole near the Bassac River and south of the field area reached bedrock at 70 m (JICA, 2002). Additionally, excavation pits near Phnom Penh, ~20 km NW of the field area, encounter bedrock at 40 m. Local well drilling, which was used to install the wells in this study, does not extend beyond 60 m depth; throughout the field area bedrock was reached only at Well PE51 in the center of the wetlands – at 40 m depth.

3.2. Surface water trends and gradients

The delta-scale gradient, as expressed by the slope of the Mekong River from Phnom Penh to the ocean, is very low, approximately 1×10^{-5} mm^{-1}. In contrast, local, seasonally-variable differences in water levels between the river and adjacent ponds and wetlands are often 2–6 m, producing gradients on the order of 1×10^{-3} mm^{-1}. As is evident in Fig. 4, the surface water levels in the river produce a seasonal signature that is similar to, but distinct from, that observed in the adjacent wetlands. The river begins rising in May or June and peaks in October at an elevation of approximately 8 m above sea level (mASL). Following a steep decline in December and January, the river continues to decline to a low of approximately 1 mASL, until the rainy season commences in June and the river again begins to rise. In contrast, wetland water levels decline through August, reaching a low at approximately 4 mASL, but then sharply rise when the river reaches flood stage in September and inundates the wetlands. Following inundation, the wetlands exhibit a rapid increase in water levels, peaking in October to approximately 7 mASL (Fig. 4).

The differences in water levels between the wetlands and the river produce significant, and seasonally-variable, gradients. The river begins rising before the wetlands and, from July through November, the river is 2–4 m higher than the wetlands. In contrast, the river falls much more rapidly than the wetlands and there is a period of approximately 8 months during which the wetlands are 2–6 m higher than the river.

3.3. Groundwater trends and gradients

Groundwater heads also exhibit dramatic seasonal variation; levels in wells fluctuate up to 8 m annually (Fig. 4). In general, groundwater levels exhibit seasonal trends that are similar, but of decreased amplitude and delayed trend arrival, to those observed in the river. In fact, seasonal changes in groundwater levels fall along a trend that lies between those observed in the wetlands and the river. Wells further from the river exhibit less seasonal variation. For example, Well TE11, which is 180 m from the river, is almost identical to river trends, experiencing ~8 m of seasonal change while Well TC31, which is 920 m from the river, varies by 7 m annually, and Well TC45, 1800 m from the river, exhibits approximately 5 m of annual head change. Comparing wetland and aquifer water levels indicates there is a strong downward gradient (2–4 m of hydraulic head difference) throughout the falling limb of the hydrograph. However, when the river is rising and higher than the wetlands, that gradient is reversed and when the river peaks, many wells across the site, particularly those in lower-elevation basins, exhibit artesian conditions, indicative of strong upward gradients.

The direction of groundwater flow within the aquifer, as expressed by observed gradients, is perpendicular to the river (Fig. 5). However, groundwater gradients between the aquifer and the river invert semi-annually; during the rising limb of the hydrograph there is gradient of approximately 10^{-3} mm^{-1} from the river into the aquifer, and when the river is falling there is a gradient of similar magnitude from the aquifer towards the river (Figs. 5 and 6).

While the gradient varies seasonally, the wetlands are higher than the river for 8 out of the 12 months of the year. Because the water levels in the river, wetlands and aquifer were measured over an entire seasonal water cycle, it is

Table 2
Material properties used in model simulations

	River	Wetland	Sand	Clay
Specific storage (m^{-1})[a]	0	5×10^{-4}	1×10^{-4}	5×10^{-4}
Porosity[b]	1	0.5	0.2	0.5
Model calibrated parameters				
Horizontal K (ms^{-1})[c]	1	1×10^{-8}	3.5×10^{-4}	1×10^{-8}
Vertical K (ms^{-1})[c]	1	1×10^{-8}	3.5×10^{-4}	1×10^{-8}

[a] Based on the literature values (Thangarajan et al., 1999; BGS and DPHE, 2001; Fleckenstein et al., 2006; Konikow and Neuzil, 2007; Masterson and Garabedian, 2007).
[b] Based on the literature values (Domenico and Schwartz, 1998).
[c] Derived from transient model calibration.

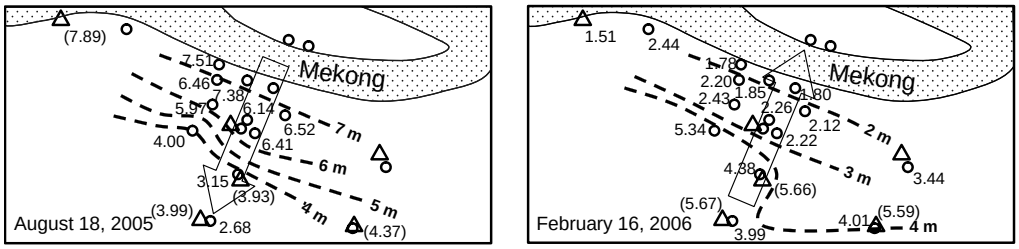

Fig. 5. Map view of hydraulic heads in wells (open circles) and surface water levels (open triangles) on August 18, 2005 (wet season) and February 16, 2006 (dry season). Numbers indicate heads in medium depth aquifer wells (20–30 m), while those in parentheses indicate surface water levels. Units reported in mASL. Dashed lines indicate hand-contoured lines of equipotential, with arrows indicating the direction of the horizontal groundwater gradient.

possible to assess the net annual gradients between these 3 water bodies. By calculating the time-weighted average of the difference in water level between the wetlands and underlying aquifer, a net annual vertical hydraulic head difference of approximately 1.2 m is obtained from the wetlands downwards into the aquifer. Similarly, comparing seasonal values for water levels in the aquifer with the adjacent river indicates a net annual hydraulic head difference of approximately 0.2 m horizontally from the aquifer towards the river. A direct comparison of the wetland levels to those observed in the river indicates an average annual head difference of 1.2–1.4 m. Importantly, these differences in hydraulic head are on the scale of decimeters to meters, while the measurement error associated with the data collection and elevation surveying is <3 cm, indicating that there is a high degree of certainty associated with these net gradient calculations; the surveying error is less than 1% of the average annual head difference between the wetlands and the river.

3.4. Aquifer hydraulic conductivity values

The measured hydraulic conductivity values for the clay range from 10^{-8} to 10^{-6} ms^{-1} and median K values range from 10^{-8} and 10^{-7} ms^{-1}, for permeameter and slug tests, respectively (Table 1). The measured hydraulic conductivity values for the sand unit range from 10^{-4} to 10^{-3} ms^{-1} with a median value of 3×10^{-4} ms^{-1} (Table 1). These values are consistent with those reported in the literature for similar sedimentary materials (Domenico and Schwartz, 1998) and are remarkably similar to the values reported for the clay aquitard and sand aquifers in Bangladesh (3×10^{-8}–9×10^{-8} ms^{-1}, and 4×10^{-4}–9×10^{-4} ms^{-1}, respectively) (Ravenscort et al., 2005).

3.5. Groundwater flux estimates

Net annual fluxes can be estimated by coupling gradients with calculated hydraulic conductivity values using Darcy's Law. Assuming an area of recharge of 25 km^2 (i.e. roughly half the field site discharges to each river) and an aquifer thickness of 45 m, a net annual gradient of ~0.065 mm^{-1}, a clay hydraulic conductivity value of 10^{-8}–10^{-7} m s^{-1}, and a porosity of 0.5, the net annual vertical flow velocity is between 0.04 and 0.4 m per year and the net annual flux downward from the wetlands to the aquifer ranges from 10^6–10^7 m^{3}a^{-1}. Independently, the flux from the aquifer to the river can also be calculated. The net annual gradient is approximately 8×10^{-5} mm^{-1}. Given the aquifer hydraulic conductivity of 10^{-4}–10^{-3} ms^{-1}, and a porosity of 0.2, net annual horizontal groundwater flow to the river ranges from 1.3 to 13 m and the net annual flux from the aquifer to the river is 10^5–10^6 m^{3}a^{-1}. The conceptual model dictates that the water that recharges the aquifer through the clay must, on an annual basis, equal the amount of water exiting the aquifer to the river. Accordingly, the actual flux through the clay is likely to be on the lower end of the calculated range while the aquifer flux to the river is on the upper end of the reported range to satisfy conservation of mass.

3.6. Net annual flow direction

Observed hydraulic gradients coupled with physically based, internally-consistent, flux calculations indicate that on an annual basis, water flows downwards from the wetlands into the underlying aquifer and horizontally from the aquifer to the river. While this would be considered a basic observation in most hydrologic settings, it is believed that this represents the first demonstration of field measurement-derived net flow direction for a regional aquifer not influenced by groundwater pumping on the deltas of Asia. This observed flow direction is consistent with the implied pre-pumping base case used in modeling of the Bangladesh system by BGS and DPHE (2001) and Klump et al. (2006). In addition, hydraulic data from a site in the Munshiganj district of Bangladesh illustrate similar patterns to those observed here except that the initiation of dry season groundwater pumping produces declines in aquifer water levels below those of the river, altering groundwater flow (Harvey et al., 2006).

3.7. Numerical model calibration

Within the transient, two-dimensional idealized flow model, a fit was obtained to the observed seasonal and daily-tidal trends in well levels by assigning hydraulic conductivity values for the sand and clay layers of 3.5×10^{-4} ms^{-1} and 1×10^{-8} ms^{-1}, respectively (Figs. 7–9). This solution is able to reproduce the general seasonal trends in water levels with increasing distance from the river and is in agreement with the flux calculations above. Simulated trends for wells immediately adjacent to the river (e.g. TC11) closely match observed trends, with well

levels showing nearly identical patterns to those in the river. At locations further from the river (TC31 and TH51), the simulated trends match the approximate 1 m decline observed in high water peak magnitude. At about a half of the more distal wells (TC51, TC45, TH71), the model underpredicts the degree of attenuation. The model results are able to capture partial attenuation of the distinct spike in July on the river hydrograph (see arrow in Fig. 4); further confirming the dominant role the river plays in dictating seasonal trends in groundwater levels.

The daily-scale tidal simulations reproduce the general observed trends with similar magnitudes in peak heights near to the river and almost complete attenuation at more distal wells (TC31). Like the seasonal trends, the tidal simulations better emulate trends closer to the river.

Importantly, the two-dimensional transient model is equally successful matching well trends along multiple transects (Fig. 8), with distance-from-the-river being sufficient to obtain simulation results similar to those observed in the field, confirming the assumption that flow is dominantly perpendicular to the river. Similarly, the model is able to reproduce trends in water levels observed in wells adjacent to the Bassac (BD11), supporting the assumption of symmetry with respect to the zone between the two rivers.

Transient model results shown in spatially distributed, cross-sectional format, also exhibit general agreement with observed trends (compare Figs. 6 and 10). The model captures the groundwater flow direction and the net gradient between the river and wetlands, but it is less successful at capturing the transient spatial distribution of the gradient; the model results for August 18th overestimate head-drop across the clay.

3.8. Net annual flow simulation

Using the net annual head differences calculated from the field data and the hydraulic conductivity values determined in the transient model, a simulation of the net annual flow field was obtained (Fig. 11). In this simulation, the observed relative head loss across the clay and sand is consistently reproduced. As illustrated by the simulated flow lines, water flows vertically downwards through the clay and nearly horizontally through the aquifer to the river. Note that the simulated results are presented with approximate vertical exaggeration of 16 times, which visually emphasizes the limited vertical component of flow in the sand. The flow velocities and travel times along the flow lines within the simulation are shown in Tables 3 and 4. Simulated travel times through the clay are on the order of 250 a, while travel times across the aquifer vary from 600 a for the most distal flow lines to less than 140 a for those close to the river. Therefore, total travel times from the wetland to the river range from about 400–900 a, values consistent with those from mass flux calculations. These flow velocities and residence times are remarkably

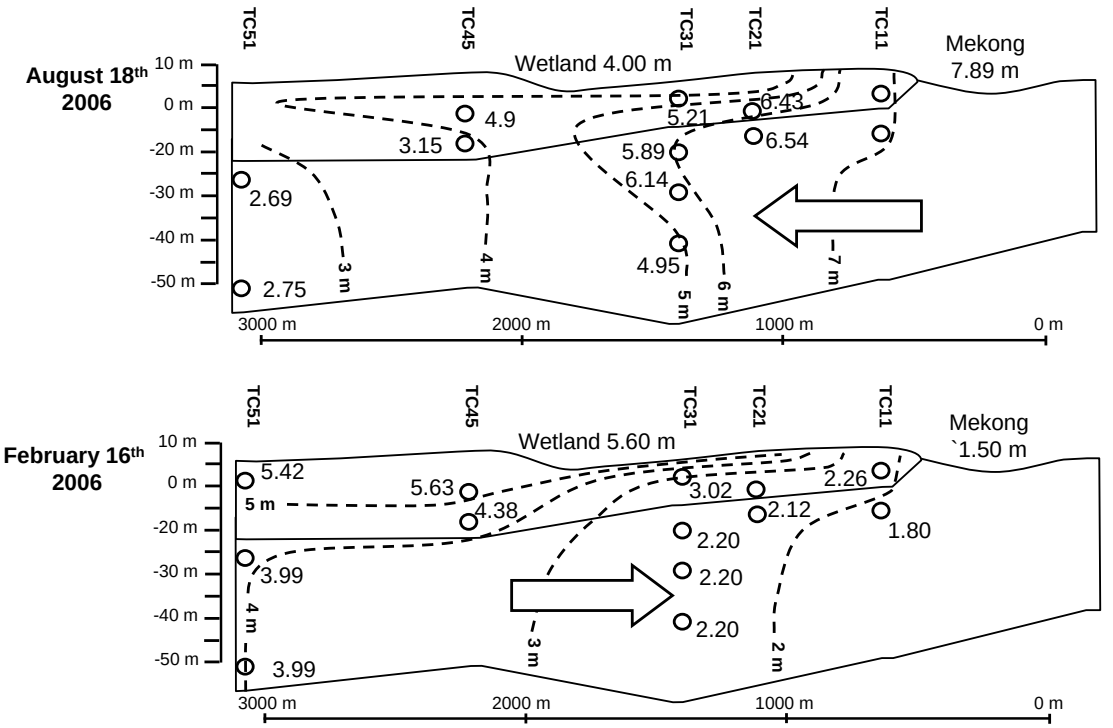

Fig. 6. Cross-sectional view (along transect depicted in Fig. 1) of hydraulic heads in wells and surface waters on August 18, 2005 and February 16, 2006, illustrating seasonal shifts in gradients. Open circles indicate well screen locations, and associated head values are in mASL. Dashed lines indicate hand-contoured lines of equal potential. Note that despite the vertical exaggeration, cross-sections are to scale.

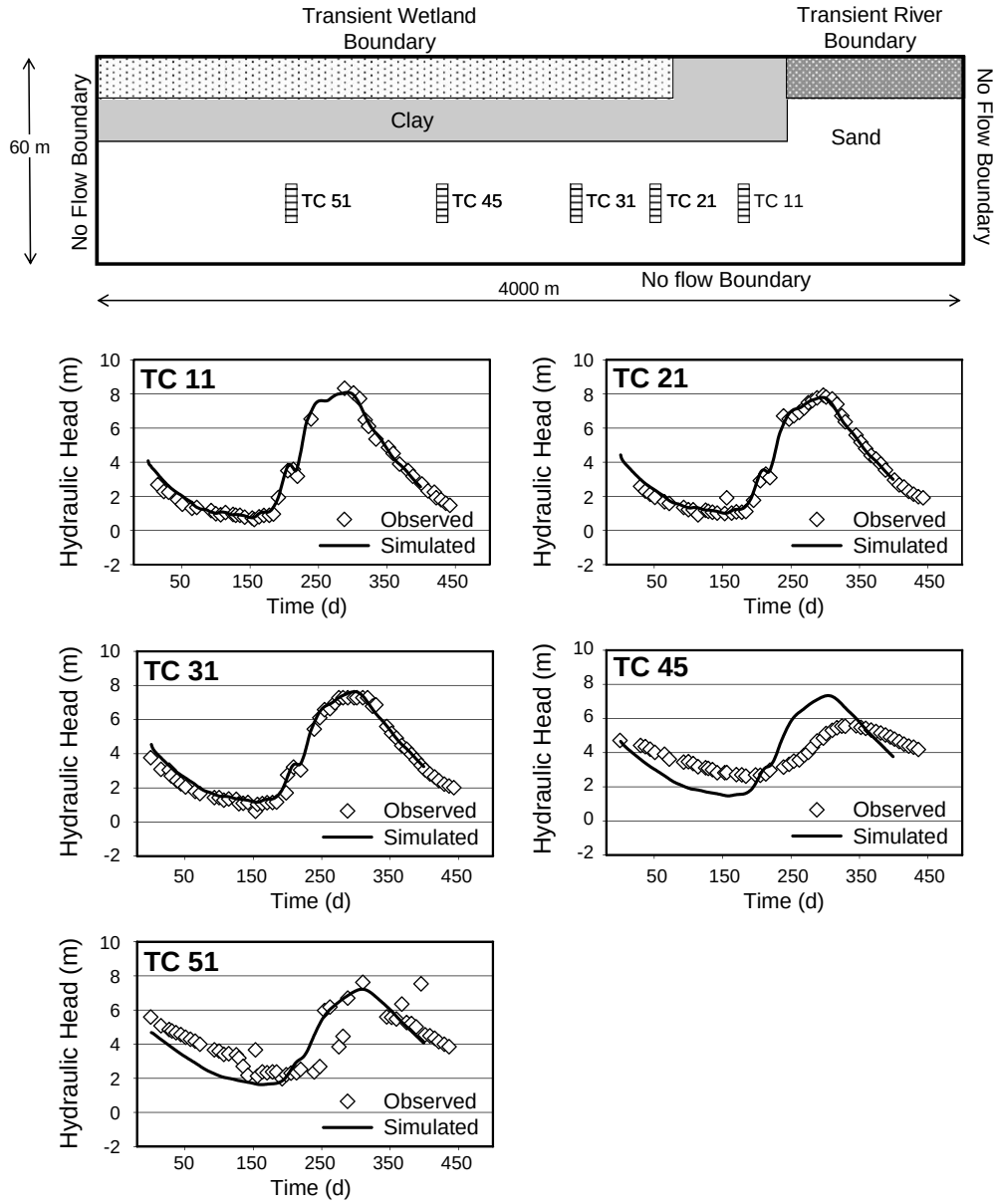

Fig. 7. Model calibration results to the TC well transect.

similar to those estimated by idealized flow modeling in Bangladesh of 300 a to travel over 1000 m under pre-pumping conditions (BGS and DPHE 2001).

3.9. Model uncertainty and utility

Given the ideality of the numerical model, it produces a remarkably good fit to observed seasonal and daily-tidal trends. Importantly, however, the modeling results remain under-constrained. In particular, the uncertainty regarding aquifer storativity values, which strongly influence the transient simulations, preclude the use of the flow modeling to markedly improve estimates of aquifer residence times over those calculated using flux estimates. The simulated flow lines are, however, independent of storativity values and are primarily dictated by the ratio of clay to sand hydraulic conductivities (a ratio well-constrained within the simulations). Therefore, the flow lines plotted in Fig. 11 provide a sound estimate of the overall, generalized net seasonal flow direction.

It is particularly noteworthy that flow lines within the clay are nearly vertical, while flow lines within the aquifer are nearly horizontal. This flow geometry suggests that tracking changes in chemistry along a vertical profile will be most effective within the upper 5–20 m of clay at this site. As those flow lines enter the underlying aquifer and are refracted to the horizontal, the uncertainty regarding individual flow paths increases. Therefore, within the

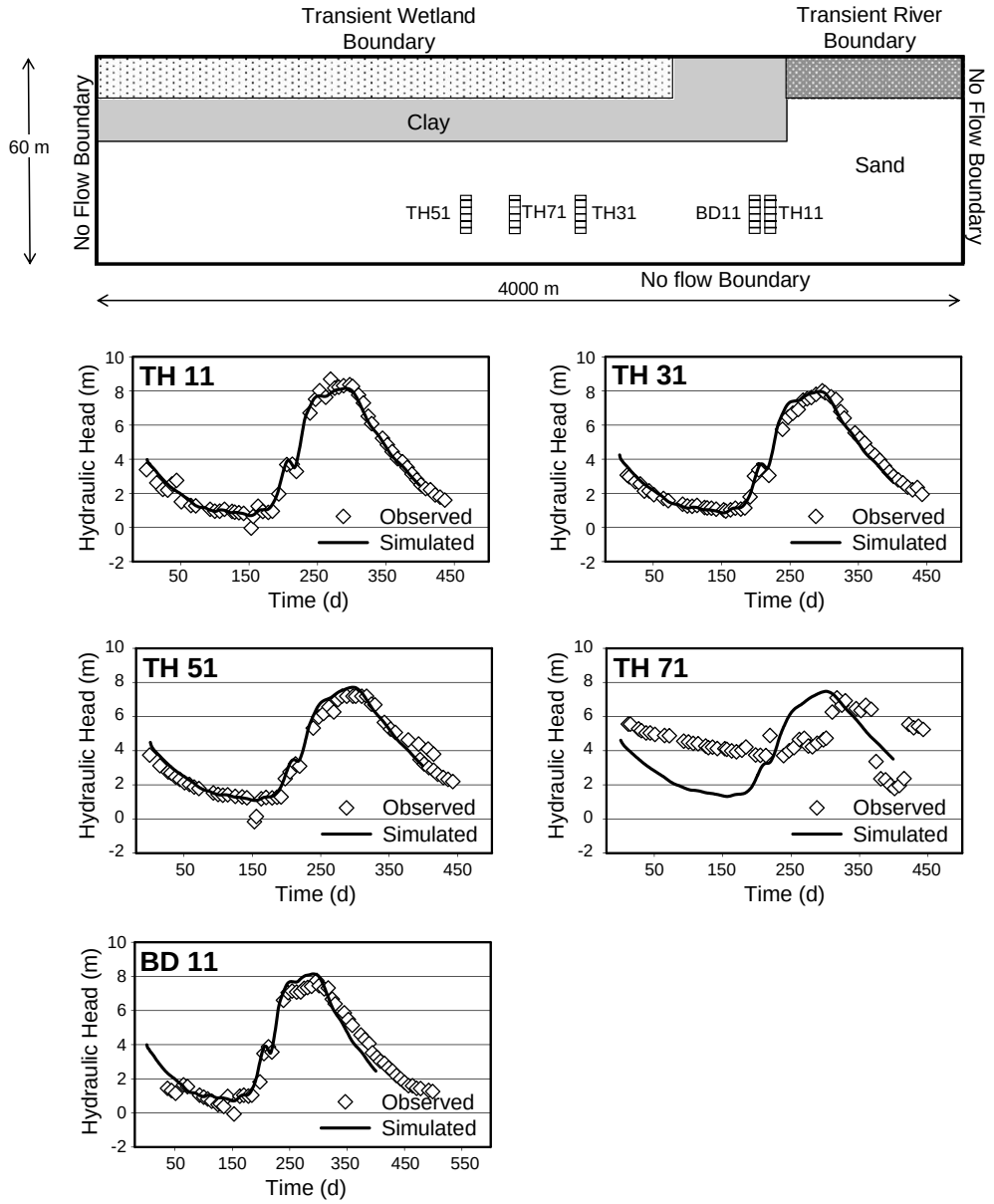

Fig. 8. Model calibration results to the TH and BD well transects.

deeper aquifer it is more appropriate to examine aquifer-scale trends in chemical parameters rather than attempting to track changes along individual flow lines.

Uncertainty regarding aquifer thickness also introduces uncertainty to model results. The base of the aquifer is estimated to be at 60 m and a number of wells at the site were drilled to depths near that range. Therefore, there is a high degree of confidence the aquifer is not significantly more shallow. The aquifer may, however, be thicker than modeled. Depth to bedrock across the region may be as deep as 160 m. If those depths exist at this site, the primary impact on model results would be an increase in the aquifer residence time and/or an increase in the model-estimated aquifer hydraulic conductivity.

While the highly idealized approach used to develop this conceptual model has proven effective at the regional scale, the local influences of hydraulic heterogeneity should not be discounted. Aquifer sediments are often highly heterogeneous, and that heterogeneity will often produce complex variations in specific flow line paths, variations that are not captured by this conceptual model. The potential impact of such heterogeneity (within the clay) is discussed below.

3.10. Potential influence of hydraulic heterogeneity

For wells TC45, TC51 and TH71, the model over-predicts drawdown during the falling limb of the hydrograph, sug-

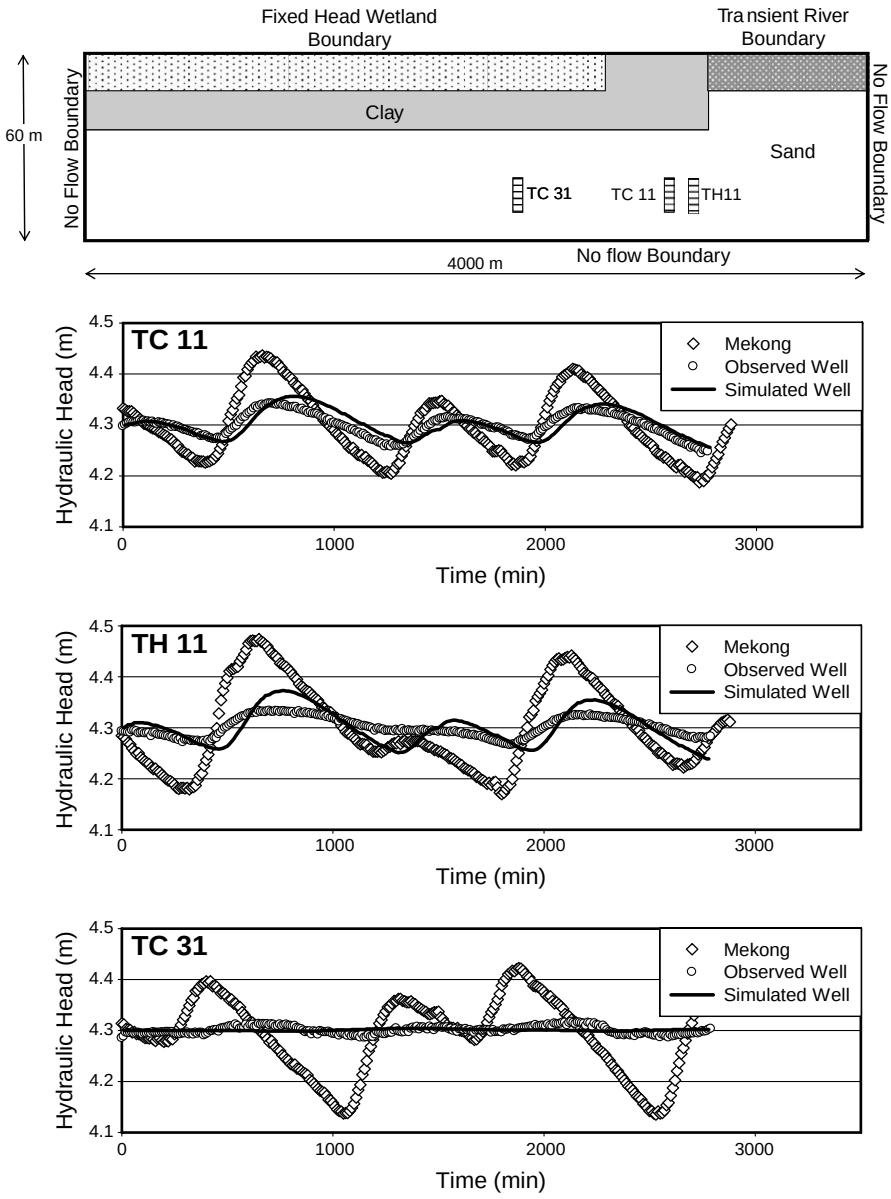

Fig. 9. Model calibration results to tidal fluctuations at TC11, TH11 and TC31. Each simulation was performed with the plotted Mekong data as a transient boundary condition and a fixed head wetland boundary. For clarity, all data was normalized to the same initial hydraulic head value of approximately 4.3 m.

gesting the limitations of the idealized model formulation. For TC45, there is also a poor match during and after the hydrograph peak. Due to appreciable logistical difficulty in collecting data during flooded conditions, later time series data for TC51 and TH71 are quite noisy; however at all three of these sites, which are located proximal to one another, the wells exhibit a seasonal trend that more closely follows that observed in the overlying wetlands (Fig. 3), suggesting increased influence of overlying surface water at these sites. To evaluate this possibility, a model simulation was performed in which the clay layer hydraulic conductivity proximal to these wells was increased to $6 \times 10^{-7}\,\mathrm{ms}^{-1}$, a change that simulates either a thinning of the clay or an increase in the hydraulic conductivity at this location (clay window, Figs. 12 and 13). This simulation produces results that improve the fit with the observed data in these three wells, indicating that spatial variations in the clay thickness or hydraulic conductivity may explain seasonal trends in these wells and may be an important feature of delta groundwater flow systems, a trend consistent with Harvey et al. (2006). Importantly, these simulations indicate that the localized zone of increased recharge influences wells some distance away (TC51 is almost 1000 m inland of the simulated high conductivity clay window), with a greater relative influence on inland wells. This simulation also highlights how preferential recharge can have a dis-

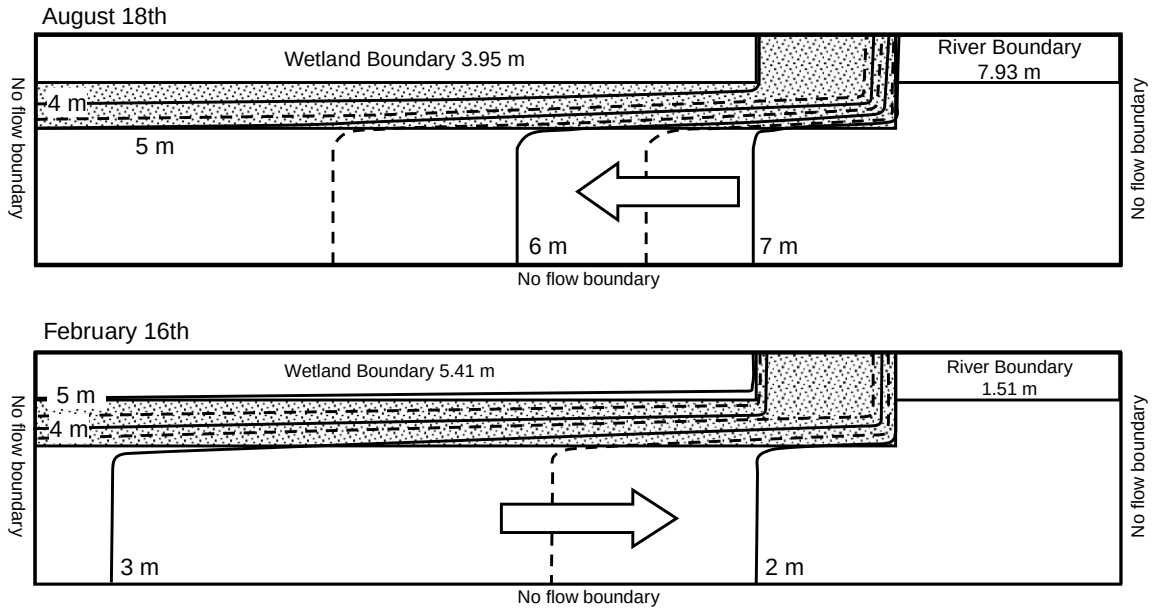

Fig. 10. Simulated hydraulic head distribution for August 18th, 2005 and February 16th, 2006. Compare to observed field values in Fig. 6.

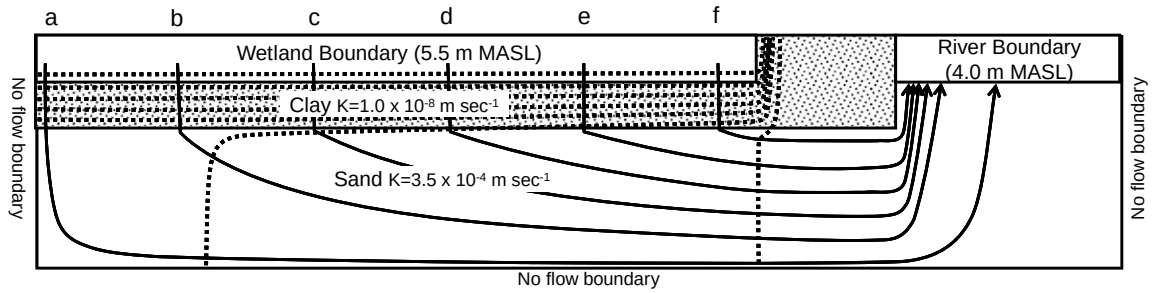

Fig. 11. Simulated flow field for net annual flow. Simulated travel times along each flow line are shown in Table 4.

Table 3
Net annual vertical and horizontal groundwater flow velocities

	Vertical flow		Horizontal flow	
	Minimum ($K = 10^{-8}$ ms^{-1})	Maximum ($K = 10^{-7}$ ms^{-1})	Minimum ($K = 10^{-4}$ ms^{-1})	Maximum ($K = 10^{-3}$ ms^{-1})
Average net flow velocity (ma^{-1})	0.04	0.43	1.3	13
Standard deviation (m)	0.003	0.034	0.87	8.8
Number of calculations	3	3	5	5

Table 4
Simulated travel times for flow paths in Fig. 11

Flow paths	Travel time (a)		
	Clay	Sand	Total
a	285	604	889
b	285	431	716
c	281	307	588
d	272	215	487
e	261	136	398
f	248	70	319

proportionate influence on flow in the subsurface; much of the aquifer water in this simulation emanates from the 'clay window'. The presence of a clay window also reduces average aquifer residence times.

3.11. Linking chemistry and net annual flow

Mapping the simulated net annual flow field on As concentrations across the aquifer (Fig. 14) provides insights on the flow-chemistry relationships, although caution should

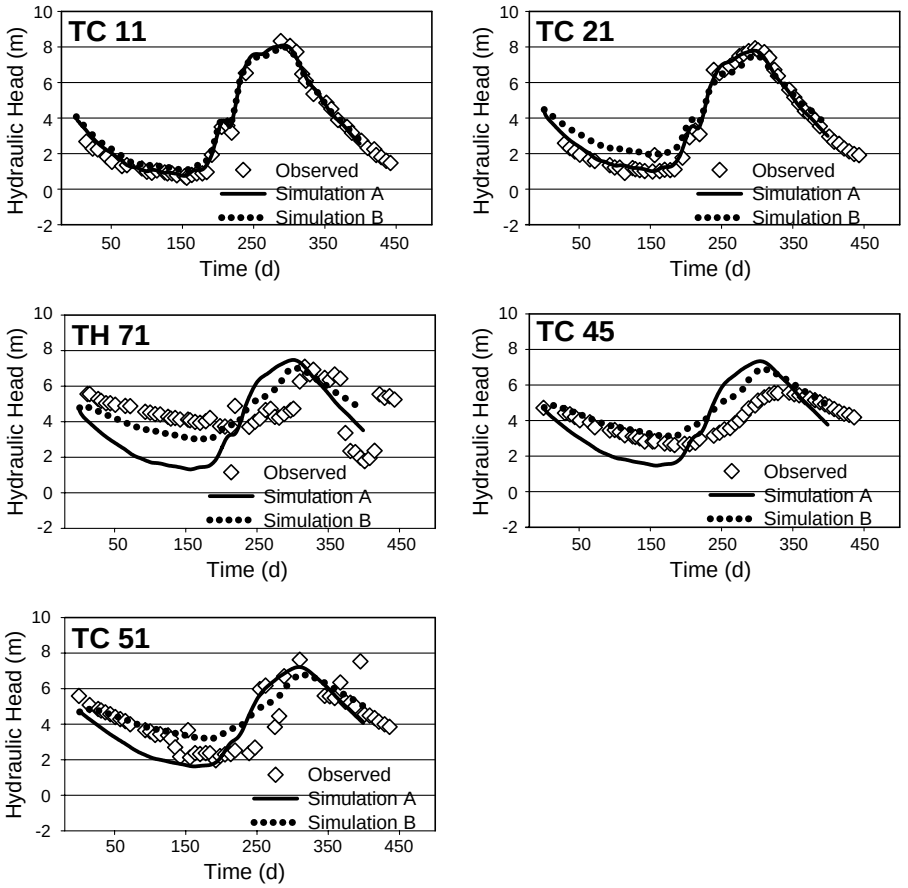

Fig. 12. Simulations with 'clay window' (dashed) and without (solid line) compared to observed trends (diamond symbols).

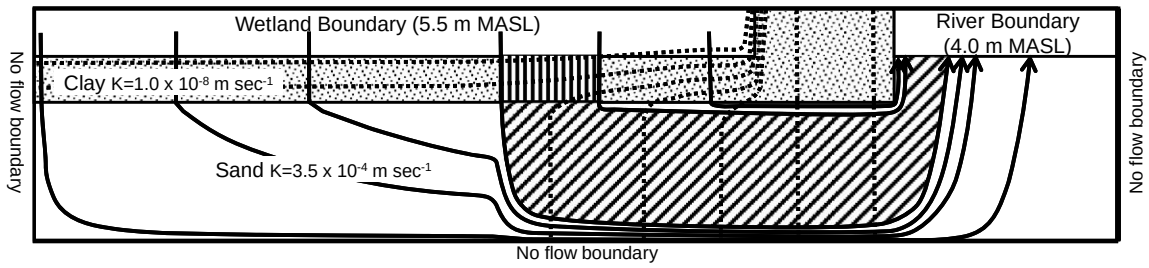

Fig. 13. Simulated flow field for net annual flow with 'clay window' (vertical hashed area, $K = 6 \times 10^{-7}\,\mathrm{ms}^{-1}$). Diagonal hashed area represents water entering the aquifer through the 'clay window'.

be used given the idealized nature of the flow simulations. Along nearly all simulated flow paths there is an increase in As concentrations with distance (age). The steepest gradients in As concentrations are, however, observed along the vertical flow lines downwards across the surficial clay sediments (concentrations increase from <1 to $500\,\mu\mathrm{g\,L}^{-1}$ over a distance of 10 m), and the highest As concentrations within the shallow pore water appear to emanate from abandoned channel pond wetlands. Detailed profiles further demonstrating gradients in As concentrations across the first 10 m of the flow path are provided and discussed in detail in Kocar et al. (2008). Increases in As concentrations along vertical profiles within the clay can be interpreted to reflect increases in As concentrations along a flow path. In contrast, within the aquifer, where flow is primarily horizontal, vertical sampling profiles will capture waters traveling along disparate flow paths with potentially very different origins and geochemical histories.

Given the estimated aquifer residence times, the deeper portion of the aquifer contains water that may be up to 1 ka and may reflect processes that occurred at some distal location under conditions that may no longer be opera-

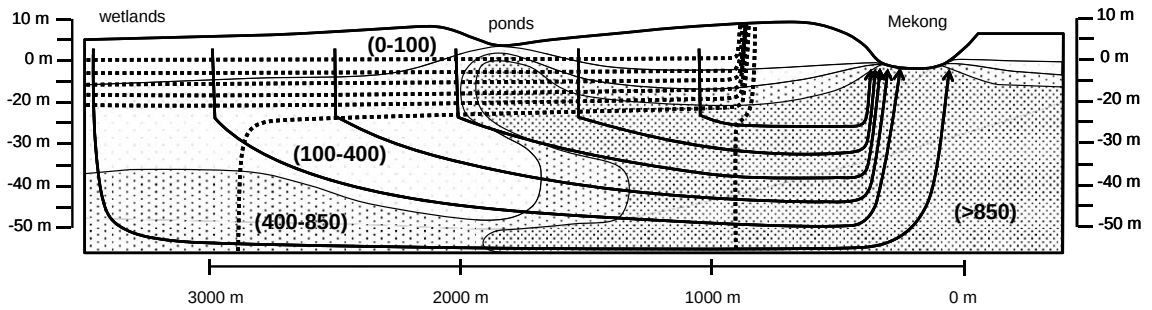

Fig. 14. Simulated flow field for net annual flow (without clay window) overlain with As concentrations. Arsenic concentrations are shown as shaded contours, and values in parentheses indicate range of intervals in $\mu g L^{-1}$.

tional today. Therefore, application of the model to trends in the deeper (and older) flow system evokes significant uncertainty. For example, at the base of the aquifer near the middle of the profile, water containing highly elevated As concentrations (>1000 $\mu g L^{-1}$) is observed. According to the conceptual model, this water entered that aquifer as recharge in the wetlands 1000 s of meters inland and 100 s of years ago and release from the sediments may have occurred at any location along that flow path. These observations suggest that the greatest certainty regarding the linkages between flow paths and processes leading to As release from sediments exists in the youngest waters flowing downwards through the surficial clay sediments.

Temporal monitoring of groundwater As concentrations indicates that seasonal variation is only observed in the zone of net recharge (shallow wells in the clay) and the zone of net discharge (at the boundary with the river). In the zone of recharge, the highest As concentrations were observed during strong downward flow, while near the river, As concentrations decline when river levels are rising and river water is flowing into the aquifer (Polizzotto et al., 2008). These trends are consistent with the proposed flow model and are indicative of relatively conservative As transport within the aquifer.

Heterogeneity in the distribution of the surficial clay would have a potentially complex influence on As distribution in the aquifer. Assuming As release is primarily from near-surface sediments, and if the release of As to the pore water is rate-limited relative to the change in infiltration velocity, a clay window could act to dilute aquifer waters (as proposed by van Geen et al., 2006). Alternatively, if the infiltrating waters also promote higher rates of As release (e.g. by providing a source of labile organic C), As concentrations in the infiltrating waters from the clay window would remain high and could be the dominant source of As to the aquifer.

3.12. Comparison with observations at other sites

Locally unique characteristics indicate that care should be taken when attempting to compare or contrast results from different research sites across the deltas of Asia. However, As-rich deltaic groundwaters of Asia share similar geologic history, topography, gross stratigraphy and dominant natural hydrologic drivers. All of these aquifers are located on massive deltaic sequences deposited over the last 10 ka. As deltaic systems, aquifer materials were similarly deposited and are composed of similar grain size distributions. At most sites throughout the deltas of Asia the aquifer materials are characterized as fine to medium grained sands with inter-bedded clays; most aquifers are capped by fine-grained silts and clays of varying thickness. All these deltaic aquifer systems are located beneath subdued, and often inverted, topography. Levees adjacent to the rivers are typically the elevation high point with inland wetland basins extending outward from the river levee system. The subdued topography, coupled with the low gradient of the river system, produces very low regional hydraulic gradients dictated by the elevation of the land surface relative to the distant ocean. In contrast, all the rivers of the Asia deltas undergo large seasonal variations in water levels (5–10 m) and, in the absence of significant groundwater extraction, these seasonal fluctuations strongly influence groundwater flow.

Direct quantitative comparisons of hydrology between deltas are limited. However, hydraulic conductivity values for both the sand and clay at this site are remarkably similar to those observed in Bangladesh (BGS and DPHE, 2001). The idealized flow-modeled velocity estimates for pre-pumping conditions in Bangladesh, are nearly identical to those obtained for the present field area (BGS and DPHE, 2001; Harvey et al., 2006). Furthermore, recent observations on the Red River, where the overlying clay layer is also thick, similarly exhibit increasing As concentrations over the clay profile (Berg et al., 2008).

Given these similarities, the first-order hydrologic characteristics observed on the upper Mekong Delta may provide a basis for understanding conditions on other deltas of Asia prior to anthropogenic disruption of the flow systems. In particular, the initial condition of groundwater flow from wetlands towards the river may prove to be a useful assumption when assessing the current complex, irrigation-influenced, flow systems observed at many sites.

An important caveat is that, while the hydrologic drivers of rising and falling rivers coupled with seasonal flooding of wetlands are similar, the amount of surficial clay across the Asian deltas varies dramatically, with some sites in Bangladesh reporting <1 m of clay compared to

up to 20 m on the Mekong Delta. Given the sensitivity of the flow system to the permeability (or thickness) of the clay aquitard, this may be a key parameter that differentiates flow behavior at sites across the deltas of Asia. Clay thickness has a particularly strong influence on aquifer residence time and the degree of vertical flow. In addition, spatial heterogeneity in clay thickness, likely to be more dramatic when the clay unit is thinner, will produce preferential infiltration, a phenomenon documented to impact As distribution in Bangladesh where the upper clay layer is sometimes absent (van Geen et al., 2006; Stute et al. 2007).

4. Summary and conclusions

The presented regional-scale hydrologic model has been calibrated against an extensive field-collected dataset and provides an internally-consistent model of water flow within the field area. The model constrains the net annual flow direction and indicates water flows downwards from wetlands through the clay aquitard and horizontally to discharge at the river. Importantly, this model provides a physical framework with which to interpret spatially distributed groundwater chemical data in the context of evolving composition over time and distance. Accordingly, observed increases in As along flow paths at this site are greatest within the vertical zone of recharge, indicating the importance of the shallow sediments as a source of As to the aquifer.

In a companion publication (Kocar et al., 2008), it is proposed that abandoned channel ponds may be particularly important sources of biogeochemical As release. Indeed, As concentration profiles align with modeled flow lines and the highest As concentrations throughout the aquifer are found along flow lines emanating from the ponds. The hydraulic behavior of wells TC45, TC51 and TH71, all proximal to but inland from the abandoned channel ponds, suggests the ponds may also produce zones of preferential recharge, potentially due to the presence of surficial deposits that are thinner or more conductive. Such a unique combination of biogeochemical and physical-hydrologic properties of abandoned channel ponds may conspire to produce both high rates of As release and high rates of recharge, potentially delivering much of the As observed in the subsurface.

Acknowledgements

This work was supported by the EVP program of Stanford's Woods Institute for the Environment, two US. EPA STAR graduate fellowships, the Stanford NSF Environmental Molecular Sciences Institute (NSF-CHE-0431425), and the Boise State University New Faculty Development Fund. We appreciate the assistance from Tom Clemo (modeling), Monty Busbee (sediment coring), Molly Meyer (surveying), Rebecca Neumann (field assistance), Amna Aziz (hydraulic conductivity determination) and the RDI staff (data collection). We would like to extend a thank you to our editor (David Polya) and reviewers (John Tellam, William Burgess, anonymous) for their helpful comments.

References

Berg, M., Stengel, C., Trang, P.T.K., Viet, P.H., Sampson, M.L., Leng, M., Samreth, S., Fredericks, D., 2007. Magnitude of arsenic pollution in the Mekong and Red River Deltas – Cambodia and Vietnam. Sci. Total Environ. 372, 413–425.

Berg, M., Trang, P.T.K., Stengel, C., Buschmann, J., Viet, P.H., Van Dan, N., Giger, W., Stüben, D., 2008. Hydrological and sedimentary controls leading to arsenic contamination of groundwater in the Hanoi area, Vietnam: the impact of iron–arsenic ratios, peat, river bank deposits, and excessive groundwater abstraction. Chem. Geol. 249, 91–112.

British Geologic Survey and Department of Public Health Engineering (BGS and DPHE), 2001. Arsenic Contamination of Groundwater in Bangladesh, Keyworth, UK.

Buschmann, J., Berg, M., Stengel, C., Sampson, M.L., 2007. Arsenic and manganese contamination of drinking water resources in Cambodia: coincidence of risk areas with low relief topography. Environ. Sci. Technol. 41, 2146–2152.

Domenico, P.A., Schwartz, F.W., 1998. Physical and Chemical Hydrogeology. John Wiley, New York.

Fleckenstein, J.H., Niswonger, R.G., Fogg, G.E., 2006. River-aquifer interactions, geologic heterogeneity, and low-flow management. Ground Water 44, 837–852.

Harvey, C.F., Swartz, C.H., Badruzzaman, A.B.M., Keon-Blute, N., Yu, W., Ali, M.A., Jay, J., Beckie, J.R., Niedan, V., Brabander, D., Oates, P.M., Ashfaque, K.N., Islam, S., Hemond, H.F., Ahmed, M.F., 2002. Arsenic mobility and groundwater extraction in Bangladesh. Science 298, 1602–1606.

Harvey, C.F., Ashfaque, K.N., Yu, W., Badruzzaman, A.B.M., Ali, M.A., Oates, P.M., Michael, H.A., Neumann, R.B., Beckie, R., Islam, S., Ahmed, M.F., 2006. Groundwater dynamics and arsenic contamination in Bangladesh. Chem. Geol. 228, 112–136.

Hvorslev, M.J., 1951. Time Lag and Soil Permeability in Groundwater Observations. US Army Corps of Engineers Waterway Experimental Station, Vicksburg, Miss.

Islam, F.S., Gault, A.G., Boothman, C., Polya, D.A., Charnock, J.M., Chatterjee, D., Lloyd, J.R., 2004. Role of metal-reducing bacteria in arsenic release from Bengal delta sediments. Nature 430, 68–71.

JICA, 2002. Assessment of Groundwater Resources in Cambodia, Kokusai Kogyo Co., Ltd.

Klump, S., Kipfer, R., Cirpka, O.A., Harvey, C.F., Brennwald, M.S., Ashfaque, K.N., Badruzzaman, A.B.M., Hug, S.J., Imboden, D.M., 2006. Groundwater dynamics and arsenic mobilization in Bangladesh assessed using noble gases and tritium. Environ. Sci. Technol. 40, 243–250.

Kocar, B.D., Polizzotto, M.L., Benner, S.G., Sampson, M., Fendorf, S., 2008. Biogeochemical and depositional controls on arsenic mobility within sediments of the Mekong Delta. Appl. Geochem. (This volume).

Konikow, L.F., Neuzil, C.E., 2007. A method to estimate groundwater depletion from confining layers. Water Resour. Res. 43, doi:10.1029/2006WR00559.

Kresic, N., 1997. Quantitative Solutions in Hydrogeology and Groundwater Modeling. CRC, Boca Raton.

Masterson, J.P., Garabedian, S.P., 2007. Effects of sea-level rise on groundwater flow in a coastal aquifer system. Ground Water 45, 209–217.

McDonald, M.G., Harbaugh, A.W., 1988. A modular three-dimensional finite-difference groundwater flow model. US Geol. Surv. Tech. Water-Resour. Invest. 34 (Book 6), 586, (Chapter A1).

McArthur, J.M., Banerjee, D.M., Hudson-Edwards, K.A., Mishra, R., Purohit, R., Ravenscroft, P., Cronin, A., Howarth, R.J., Chatterjee, A., Talukder, T., Lowry, D., Houghton, S., Chadha, D.K., 2004. Natural organic matter in sedimentary basins and its relation to arsenic in anoxic groundwater: the example of West Bengal and its worldwide implications. Appl. Geochem. 19, 1255–1293.

Nguyen, V.L., Ta, T.K.O., Tateishi, M., 2000. Late holocene depositional environments and coastal evolution of the Mekong River Delta, Southern Vietnam. J. Asian Earth Sci. 18, 427–439.

Nickson, R.T., McArthur, J.M., Ravenscroft, P., Burgess, W.G., Ahmed, K.M., 2000. Mechanism of arsenic release to groundwater, Bangladesh and West Bengal. Appl. Geochem. 15, 403–413.

Polizzotto, M.L., Harvey, C.F., Sutton, S.R., Fendorf, S., 2005. Processes conducive to the release and transport of arsenic into aquifers of Bangladesh. Proc. Nat. Acad. Sci. USA 102, 18819–18823.

Polizzotto, M.L., Kocar, B.D., Benner, S.G., Sampson, M., Fendorf, S., 2008. Near-surface wetland sediments as a source of arsenic release to ground water in Asia. Nature 454, 505–508.

Polya, D.A., Gault, A.G., Diebe, N., Feldman, P., Rosenboom, J.W., Gilligan, E., Fredericks, D., Milton, A.H., Sampson, M., Rowland, H.A.L., Lythgoe, P.R., Jones, J.C., Middleton, C., Cooke, D.A., 2005. Arsenic hazard in shallow Cambodian groundwaters. Miner. Mag. 69, 807–823.

Postma, D., Larsen, F., Hue, N.T.M., Duc, M.T., Viet, P.H., Nhan, P.Q., Jessen, S., 2007. Arsenic in groundwater of the Red River floodplain, Vietnam: controlling geochemical processes and reactive transport modeling. Geochim. Cosmochim. Acta 71, 5054–5071.

Ravenscort, P., Burgess, W.G., Ahmed, K.M., Burren, M., Perrin, J., 2005. Arsenic in groundwater of the Bengal Basin, Bangladesh: distribution, field relations, and hydrological setting. Hydrol. J. 13, 727–751.

Stute, M., Zheng, Y., Schlosser, P., Horneman, A., Dhar, R.K., Hoque, M.A., Seddique, A.A., Shamsudduha, M., Ahmed, K.M., van Geen, A., 2007. Hydrological control of As concentrations in Bangladesh groundwater. Water Resour. Res. 43, doi:10.1029/2005WR00449 W09417.

Ta, T.K.O., Nguyen, V.L., Tateishi, M., Kobayashi, I., Tanabe, S., Saito, Y., 2002. Holocene delta evolution and sediment discharge of the Mekong River southern Vietnam. Quatern. Sci. Rev. 21, 1807–1819.

Tamura, T., Saito, Y., Sieng, S., Ben, B., Kong, M., Choup, S., Tsukawaki, S., 2007. Depositional facies and radiocarbon ages of a drill core from the Mekong River lowland near Phnom Penh, Cambodia: evidence for tidal sedimentation at the time of holocene maximum flooding. J. Asian Earth Sci. 29, 585–592.

Thangarajan, M., Linn, F., Uhl, V., Bakaya, T.B., Gabaake, G.G., 1999. Modelling an inland delta aquifer system to evolve pre-development management schemes: a case study upper Thamalakane River valley, Botswana, southern Africa. Environ. Geol. 38, 285–295.

van Geen, A., Aziz, Z., Horneman, A., Weinman, B., Dhar, P.K., Zheng, Y., Goodbred, S., Versteeg, R., Seddique, A.A., Hoque, M.A., Ahmed, K.M., 2006. Preliminary evidence of a link between surface soil properties and the arsenic content of shallow groundwater in Bangladesh. J. Geochem. Explor. 88, 157–161.